International Journal of Research Available at https://edupediapublications.org/journals
e-ISSN: 2348-6848
p-ISSN: 2348-795X
Volume 03 Issue 5
March2016

Fatigue and fracture behaviour of plain Concrete (High-cycle fatigue of notched plain concrete

V Srikanti[1], U Venkata Ratnam[2]
[1] B. Tech Scholar, Department of Civil Engineering, Siddhartha Institute of Engineering and Technology, Vinobha Nagar, Ibrahimpatnam, Hyderabad, Telangana 501506.
[2]Asst. Professor, Department of Civil Engineering, Siddhartha Institute of Engineering and Technology, Vinobha Nagar, Ibrahimpatnam, Hyderabad, Telangana 501506

Abstract

This paper investigates the accuracy of the so-called Theory of Critical Distances (TCD) in modelling, in the high-cycle fatigue regime, the behaviour of notched plain concrete. The TCD postulates that the fatigue damage extent has to be estimated by directly post-processing the entire linear-elastic stress field damaging the material in the vicinity of the crack initiation locations. According to the TCD's modus operandi, the high-cycle fatigue assessment is performed by using a scale length parameter which is treated as a material property. The accuracy of this method was checked against a number of experimental results generated by testing, under four-point bending, notched specimens of plain concrete. This validation exercise allowed us to prove that the TCD is successful in estimating the high-cycle fatigue strength of notched concrete beams, resulting in predictions falling within an error interval of about ±15%

Keywords: plain concrete, fatigue, notch, Theory of Critical Distances

I. Introduction

In situations of practical interest concrete structures can undergo in-service time-variable loading. This is a common situation, for instance, in runways subjected to repeated loads due to passing aircrafts, asphalt concretes subjected to cyclic local pressures resulting from the action of tyres, and the concrete structural parts of bridges cyclically loaded by traveling motor vehicles. Even though, since the beginning of the last century (Von Ornum, 1903; Von Ornum, 1907) a tremendous effort has been made by the international scientific community, examination of the state of the art shows that a universally accepted strategy suitable for efficiently perform the fatigue assessment of concrete has not been agreed yet. Further, other than a few isolated investigations (Ohlsson et al.

1990; Plizzari et al., 1997; Thun et al., 2011), no systematic work has been carried out so far in order to devise specific methods capable of taking into account the detrimental effect of notches weakening plain concrete structural details subjected to in-service fatigue loading. In this challenging scenario, the present paper reports on an attempt of using the so-called Theory of Critical Distances (TCD) to perform the high-cycle fatigue assessment of notched plain concrete.

Due to the heterogeneous nature of concrete and its inherent flaws (e.g. pores, water inclusions, microscopic cracks due to shrinkage, etc.), its failure mechanism essentially involves a rather complex process of crack formation and crack growth [1]. Typical phenomena, such as softening behaviour, caused by distributed cracking, transition of micro-cracks to macro-cracks prior to failure, and bridging stresses along the fracture process zone (FPZ1) can be explained by applying NLFM 2 [2]. In order to do so, the experimental determination of several fracture parameters is required. Even though no standardized test methods exist, the 3PBT3 and the WST4 on notched specimens are commonly used [3]. The inevitable macro-cracking mechanism in concrete structures, caused by the coalescence of microscopic imperfections, may seriously affect the aesthetic look, but may also jeopardize the

construction's stability. Hence it is crucial to fully understand the fracture behaviour of the different concrete types used worldwide in the civil engineering industry. Since VC5 and SCC6 have a significantly different mix design different material characteristics are affected, as well. Already a considerable amount of research has been carried out on the fresh, mechanical and transport properties and on the durability of SCC [4–6], showing some remarkable. Differences, compared to VC. For instance, the higher content of fine particles (e.g. by adding fillers) influences the whole microstructure, making the interfacial transition zone of SCC stronger and consequently increasing the compressive and tensile strength, compared to VC with similar w/c ratio [4]. Furthermore, the reduction in the amount of coarse aggregates in SCC contributes to a lower stiffness, when compared to VC of equal strength [7]. As a result, a distinct fracture behaviour of both concrete types can be expected, for it is both, the strength of the cement paste, and the location and size of the aggregates that play an important role regarding crack resistance [8,9]. Therefore, in this study 3PBTs and WSTs are performed, both statically and dynamically, on samples, made from VC and two SCC mixtures (one with similar compressive strength and another with equal w/c ratio). The static and dynamic fracture parameters, obtained from these experiments, allow to interpret and compare the cracking behaviour of the different concrete types.

II. Materials and methods

Concrete mixtures

Table 1 displays the concrete compositions used in this study. They were provided by a ready-mix concrete company. VC, a traditional vibrated concrete mix, functions as a reference for comparison with two self-compacting concrete mixtures: one with similar compressive strength (SCC1) and another with equal w/c ratio (SCC2). As can be seen, the cement type and the aggregate sizes are identical for the three mixtures, thereby excluding these as possible influencing factors for the cracking resistance. Different experiments were performed on the freshly-mixed concrete batches. First, the air content was measured using the pressure method as described in the European Standard EN 12350-7 [10]. Additionally, workability tests were carried out to ensure a good consistency and a proper filling ability of the formwork. In case of VC, slump and flow tests were performed, according to EN 12350-2 [11] and EN 12350-5 [12], respectively. Both SCC mixtures underwent slump-flow tests and V-funnel tests, defined in EN 12350-8 [13] and EN 12350-9 [14]. All the results are displayed in Table 2. Afterwards, per batch several beams and wedge-splitting samples were cast, along with at least six control specimens (cubes with side 150 mm and cylinders with diameter 150 mm and height 300 mm) in order to determine the compressive strength of each concrete type. After a sealed curing period of 24 h, these standardized cubes and cylinders were demoulded and stored under water at 20 ± 2 C. Then, they were tested at different ages, following the guidelines of EN 12390-3 [15]. fcm represents the mean value of the cylindrical compressive strength, fc,cub,m is the average cubical compressive strength, and the index 'k' is used to indicate the corresponding characteristic values. Based on the resulting strengths at 28 days, the average tensile strength fctm was calculated by Eq. (1) [16]. Furthermore, Young's modulus Ecm was obtained experimentally by deformation measurements on axially, in compression loaded cylinders of diameter 150 mm and height 300 mm, according to the National Belgian Application Document NBN B15-203 [17]. These findings are also listed in Table 2. fctm ¼ 0:3f 2 3 ck ð1Þ The consistency classes, shown in Table 2, demonstrate a sufficiently fluid and workable character for all of the three concrete mixtures. Hence, no problems regarding workability or compaction during casting were reported. When considering the air content, the highest value is noticed in case of VC, followed by SCC2 and SCC1, respectively. The results of the compressive strength measurements, however, are not affected by these different amounts of air, since VC and SCC1 show a similar strength (class C35/45, as was aimed for), whereas SCC2 is classified in

Table 1: Concrete compositions.

COMPOSITION	VC (kg/m^3)	SCC1 (kg/m^3)	SCC2 [kg/m^3]
CEM III/A 42.5 LA	360	293	360
Water	161	161	161
Sand 0/4	759	651	651
Crushed limestone 2/6.3	433	523	523
Crushed limestone 6.3/14	610	321	321
Limestone filler	0	377	317
Superplasticizer (PCE)	2.7	9.0	9.5
Retarding agent	1.2	0.0	0.0

The higher strength class C45/55 (as could be expected). The values of Young's modulus for VC and SCC1 are comparable. In case of SCC2, the large variation does not allow to draw clear conclusions concerning its Young's modulus. SCC2 does show the largest tensile strength, followed by VC and SCC1, for which the values are similar.

III. Specimens

Three-point bending test specimens

The 3PBT specimens were cast in beam-shaped moulds with dimensions 100 100 400 mm (see Fig. 1), and sealed for 24 h. After demoulding, they were stored in lab conditions for about five months. Approximately two days before testing, a notch of width 3 mm was made in the middle of the beam's side surface, using a wet diamond saw. This way, a smooth top and bottom surface could be assured. According to RILEM recommendations the notch depth must be 1/3rd of the beam's height in order to ensure the location of crack initiation. Consequently, the notch length was chosen 33 mm.

Wedge-splitting test specimens

The geometry and dimensions of the cubical WST specimens, as depicted in Fig. 2, are based on the findings of Löfgren et al. Additional information and other dimensions can be found. The samples were made using a standard cube mould (side 150 mm), into which a wooden bar with rectangular section (30 22 mm) was placed. The bar was attached to the side of the mould in order to obtain a plain top surface with guiding groove. After sealed curing for 24 h, the specimens were demoulded and also stored in lab conditions for several months. Again, two days prior to testing, a 3 mm wide and 33 mm long starter notch was cut by wet diamond sawing.

Test procedure

Three-point bending test

Fig. 3 illustrates the 3PBT setup for both static and dynamic tests, where a vertical, linear load was applied onto the middle of the beams' top surface, using a compression test device. With the beams resting on two line supports with a span length of 300 mm, the specimens started cracking at the notch tip as the load increased. During the entire loading process, the load (F) was continuously registered with a computer controlled data acquisition system and the opening of the notch or the crack mouth opening displacement (CMOD) was measured by a clip gauge. In case of the static tests, a constant increment rate of the CMOD of 0.0005 mm/min was applied. The dynamic tests were conducted load-controlled with a speed of 1.5 kN/s resulting in a frequency of approximately 0.33 Hz. The lower limit of the sinusoidal load function was chosen 10% of the average static ultimate load, for the upper limit various percentages were selected: 90%, 80%, 75% and 70 %.

Wedge-splitting test

For the WSTs, the concrete cubes were placed onto a steel plate with two linear supports. At the top, the compression test device applied a vertical, static or dynamic load onto a transfer beam with two metal wedges (angle 30). These wedges move between two roller bearings, mounted on two metal caps, which rest on the edges of the specimen's guiding groove (Fig. 4). The vertical displacement (F_v) was thus transformed into two horizontal splitting forces (F_{sp}), which caused the specimen to crack, also starting at the notch tip.

International Journal of Research Available at https://edupediapublications.org/journals
e-ISSN: 2348-6848
p-ISSN: 2348-795X
Volume 03 Issue 5
March2016

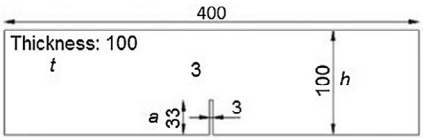

Fig. 1. 3PBT specimen's geometry and dimensions (mm).

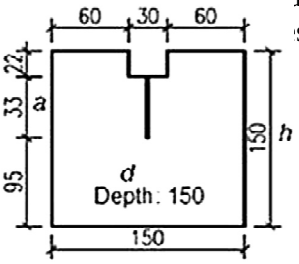

Fig. 2. WST specimen's geometry and dimensions (mm).

Again, the load (F_v) was continuously recorded with a computer controlled data acquisition system and a clip gauge, mounted at the top of the guiding groove, registered the evolution of the CMOD. Controlled downward movement of the wedges for the static experiments was created by setting the testing machine in CMOD mode and a speed of 0.0005 mm/min was applied. The load-controlled dynamic tests were again conducted by applying a sinusoidal function with a frequency of about 0.33 Hz and equal minimum and maximum load levels as in case of the 3PBT (i.e. 10–90%, 10–80%, 10–75%, and 10–70%).

IV. Calculation methods

Fracture parameters

Based on the experimentally obtained load–CMOD curves of the static tests, the fracture energy $G_{F1,exp}$, representing the total energy dissipation during the cracking process, was calculated by Eq. (2). In case of the 3PBT, F equals the recorded vertical load F_v, whereas for the WST, the splitting force F_{sp} must be determined by Eq. (3). Normally, the friction of the roller bearings should be accounted for, but the friction coefficients, provided by manufacturers, range from 0.1% to 0.5% and lead to an effect on the splitting force of only 0.4% to 1.9%, which may be neglected. The characteristic length $l_{ch,exp}$, as given by Eq. (4) from Hillerborg's cohesive crack approach, is a unique material property and expresses the brittleness of the concrete specimens. The lower the value, the more brittle the material. Another indicator for the material's brittleness, the critical stress intensity factor $K_{Ic,exp}$ (also from the cohesive crack theory), was determined by using Eq. (5). The index ''exp'' is added to emphasize the fact that these parameters are extracted from the experimental results.

$$G_{F,exp} = \frac{1}{(h-a)d}\int Fd(CMOD)$$

$$F_{sp} = \frac{F_V}{2\tan\frac{\alpha}{2}}$$

$$l_{ch,exp} = \frac{EG_F}{f_t^2}$$

$$K_{Ic,exp} = \sqrt{EG_F}$$

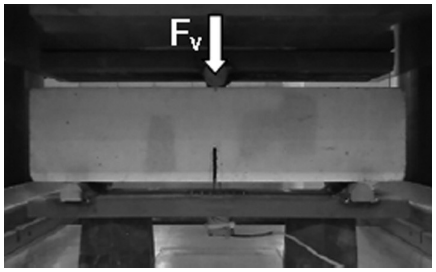

Fig. 3. Three-point bending test setup.

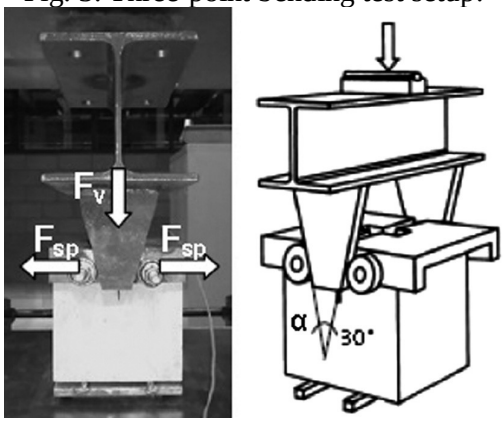

Fig. 4. Wedge-splitting test setup.

Inverse analysis

Inverse analysis of the experimentally obtained load–CMOD curve – also referred to as parameter or function estimation – can be used for determining the non-linear fracture parameters of concrete, based on the 3PBT or WST results. The principle (see Fig. 5) consists in minimizing the differences between the calculated displacements and the displacements obtained from the experimental data (e.g. CMOD), thus allowing to define the relationship between the stress r and the crack opening w, the so-called softening curve. Extensive research on regular concrete has resulted in various approaches and different r-w curves (non-linear, bilinear, multilinear). The strategy used in this study is based on the so-called hinge model, in which the parameters (f_t, a_1, a_2, and b_2) of a bilinear stress-crack opening relationship (Fig. 5) are calculated, after estimating Young's modulus E. The assumption that the presence of the crack changes the stress and strain field only locally and lets the rest of the structure unaffected, benefits the computational cost and simplicity of the model.

Besides generating the softening curves, the inverse analysis code also assesses different fracture parameters; the total fracture energy $G_{F,calc}$, the initial fracture energy $G_{f,calc}$ (corresponding with the area under the first, steep sloped line of the bilinear curve and representing the energy release before the peak load is reached), the characteristic length $l_{ch,calc}$, and the stress intensity factor $K_{Ic,calc}$. Here, the index ''calc'' denotes the fact that these values originate from numerical computation software.

V. Results and discussion

Three-point bending test

Load–CMOD curves

From the experimentally obtained load–CMOD curves of all specimens, the average curves for VC (12 specimens), SCC1 (10) , and SCC2 (11), acquired by calculating the mean force at fixed CMOD values, are displayed in Fig. 6. The thinner lines outline the accompanying 90% confidence interval. A summary of the peak loads (P_{max}) and the corresponding CMOD values is also provided in Table 3. It can be seen that the sharpest peak appears in the curve of SCC1, with the highest maximum load occurring at the smallest CMOD. VC and SCC2 show a similar behaviour, which differs from that of SCC1. This can be attributed to the higher w/c ratio (0.55), compared to the other batches (0.45), because the higher the water content, the weaker the interfacial transition zone, which affects the cohesive properties of the paste. Less stresses are transmitted across the crack due to an attenuated wedging mechanism and an intensified pull-out behaviour of the aggregates.

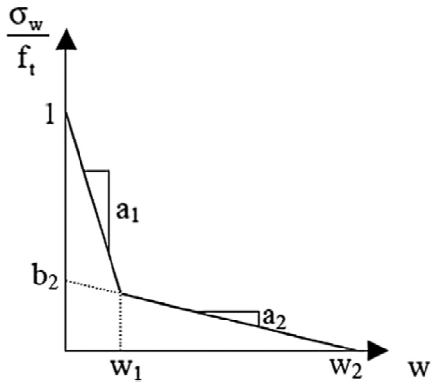

Fig. 5. Parameters of bilinear softening curve.

Table 3 lists the results of the fracture parameters, calculated by Eqs. (2), (4), and (5) from paragraph 3.1. It is clear that the beams made from SCC1 (with the highest w/c ratio and thus the weakest cement paste), have the smallest cracking resistance, since they generate the lowest values for $G_{F1,exp}$, $l_{ch,exp}$, and $K_{Ic,exp}$ (see Table 3). This means that SCC1 is the most brittle of the three mixtures and that less energy is released during fracture, when compared to VC and SCC2. Moreover, the peak load is reached earlier (at a lower CMOD value).

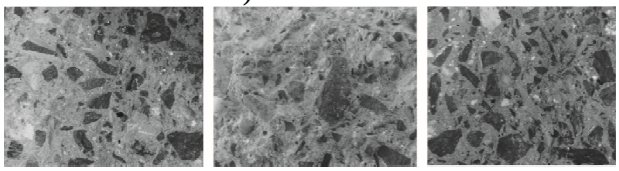

Fig. 6. Average load–CMOD curves for 3PBT (VC, SCC1, SCC2).

As also indicated by Petersson, aggregate pull-out plays an important role in the 3PBT setup. In case of a high w/c ratio (and thus a weak cement paste), the aggregates will experience pullout instead of fracture, resulting in a decrease of the fracture energy. The fracture patterns of the different mixtures, as displayed in Fig. 7, affirm that statement.

Fatigue resistance

As shown in Table 5, the number of cycles to failure increases as the upper load limit in the dynamic tests decreases. For all applied load levels, SCC2 shows the best fatigue resistance, compared to the other mixtures. SCC1, which turned out to be the most brittle in the static tests, performs worst. This relationship seems to correspond with the values of the compressive strength, which is the largest in case of SCC2 and the smallest for SCC1 (although there is little difference with VC). Figs. 9–12 display the evolution of the CMOD as a function of the number of cycles for the different load limits. As stated by Horii et al., the mechanism of fatigue crack growth under cyclic loading generally consists of an initiation phase and a propagation phase. The micro-crack initiation is dominant in the beginning and is followed by a stable propagation period until a macro-crack is formed, which grows rapidly up to failure. Since in the conducted tests an existing crack is present by means of a notch, only the propagation stage (with a slowly ascending part and a subsequent quickly growing part) is visible in the graphs. Notice that the slope of the CMOD growth curve becomes steeper and the number of cycles in the final phase becomes smaller as the load level increases.

It needs to be mentioned that the specimens, which failed after only one load cycle, were probably subjected to a higher load level than intended, because their static failure load presumably would have been lower than the mean value of the actual conducted static tests. Indeed, when comparing the average static load–CMOD curve to the dynamic ones, it is noticed that the CMOD values, corresponding to the maximum applied load level of these dynamically tested specimens, already exceed the CMOD value at peak load of the static curve. Due to the large deformations occurring in the latter's descending branch and the substantial decrease in stiffness, certain specimens prematurely fail after one dynamic load cycle. This inevitable phenomenon is related to the heterogeneous nature of concrete, causing a large spread in the strength of different samples.

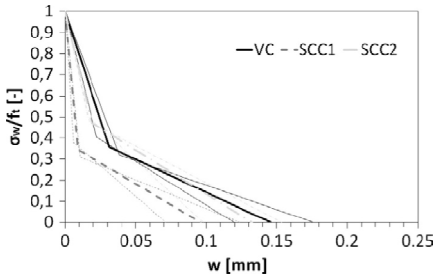

Fig. 7. Average softening curves for 3PBT (VC, SCC1, SCC2).

Table 2: Average parameters inverse analysis for 3PBT (VC, SCC1, and SCC2).

	VC (average)	SCC1 (average)	SCC2 (average)
a1 (mm1)	20.65	72.34	28.19
a2 (mm1)	3.12	3.96	4.16
b_2 (–)	0.46	0.38	0.55
f_t (MPa)	4.40	6.61	4.57
E (MPa)	28,300	40,800	29,300
$G_{F,calc}$ (N/m)	183	140	186
$l_{ch,calc}$ (mm)	268	130	261
DP (%)	1.75	1.74	1.49

Table 3: Fatigue resistance for 3PBT (VC, SCC1, andSCC2).

	VC (# cycles)	SCC1 (# cycles)	SCC2 (# cycles)
10–90%	1	1	8
10–80% A	2	2	3
10–80% B	1	3	39
10–75%	31	7	65

10–70% A	25	3	404
10–70% B	51	18	677

Wedge-splitting test

Load-CMOD curves

The average load–CMOD curves and their 90% confidence intervals in Fig. 13, obtained from the WSTs, show a good agreement between SCC1 and SCC2 and a somewhat different behaviour for VC. The peak loads, which are also summarized in Table 6, do not remarkably differ. Only the CMOD value at peak load is slightly larger in case of VC. However, it is clear that, compared to the load–CMOD curves from the 3PBT, an altered mutual relationship between the three concrete types is found.

Softening curves

As to the softening curves in Fig. 14, derived from the load– CMOD curves of Fig. 13, likewise a good correspondence is noticed between the SCC1 and SCC2. Less pre-peak damage occurs and less pre-peak energy is dissipated, when compared to VC, which can be explained by the higher tensile stress in Table 7 (obtained from inverse analysis). But again, the values for f_{ctm} in Table 2 (based on the characteristic compressive strength of the mixtures) show a substantially different relationship. However, the DP values of Table 7, being similar and minimal, demonstrate reliable inverse analysis outcome for all WSTs. Also the total fracture energy is the smallest for the SCC batches and the characteristic length the largest (see Table 7), confirming them to be the most brittle of the three tested concrete types. Analogous G_F values are found from WSTs on normal concrete specimens. The characteristic length, on the other hand, is again too large, compared to the results in Table 7, but this can be attributed to a substantially smaller E-value, in combination with a considerably larger tensile strength, compared to the values in Table 7.

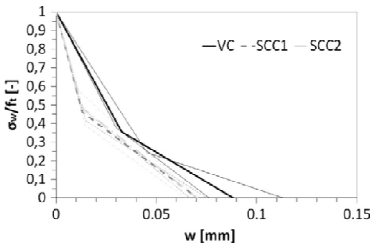

Fig. 8. Average softening curves for WST (VC, SCC1, SCC2).

Table 4: Average parameters inverse analysis for WST (VC, SCC1, and SCC2).

	VC (average)	SCC1 (average)	SCC2 (average)
a1 (mm1)	19.64	41.20	38.81
a2 (mm1)	6.39	8.02	8.45
b_2 (–)	0.57	0.57	0.60
f_t (MPa)	4.55	5.05	4.93
E (MPa)	31,900	39,300	38,200
$G_{F,calc}$ (N/m)	146	115	117
$l_{ch,calc}$ (mm)	226	178	184
DP (%)	1.40	1.54	1.41

Table 5: Fatigue resistance for WST (VC, SCC1, and SCC2).

	VC (# cycles)	SCC1 (# cycles)	SCC2 (# cycles)
10–90% A	368	7	743
10–90% B	271	334	726
10–80%	13,088	2066	545
10–75% A	77,409	7061	11,002
10–	/	384	/

75%
B

10–70%	110,941	1168	3099

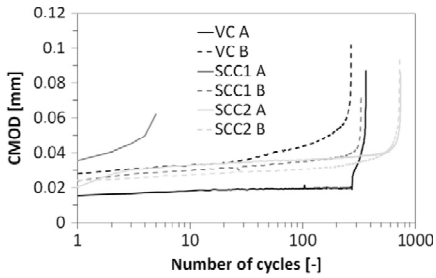

Fig. 9. Evolution of CMOD during dynamic WST with limits 10–90% (VC, SCC1,SCC2).

Experimental vs. numerical parameters

As already reported in Sections 4.1.3 and 4.2.3, the numerically obtained parameters (f_t, E, G_F, and l_{ch}) from the inverse analysis substantially deviate from those based on the experimental load–CMOD curves. In case of the 3PBT, the largest differences are found for l_{ch}, whose calculated values are on average 53% smaller than the experimentally determined ones. $G_{F,exp}$ is approximated best by the inverse analysis, with an underestimation of only 9%. For the
WST, on the other hand, $l_{ch,calc}$ is only 15% smaller than $l_{ch,exp}$, while the numerical fracture energy is overestimated with 47%. In both test setups, the inverse analysis also consistently yields larger values for the tensile strength. Moreover, the mutual relationship between the three concrete types is altered: the highest value occurs in case of SCC1, whereas f_{ctm} is largest for SCC2. Regarding Young's modulus, the best agreement with the experimental outcome is present for SCC1, for the 3PBT as well as the WST.

VI. Conclusions

As a general conclusion from the static three-point bending tests (3PBTs) and wedge-splitting tests (WSTs), it can be stated that the self-compacting concrete type with similar strength as the vibrated concrete mix (SCC1) is the most brittle concrete type, due to the higher w/c ratio and thus the weakest cement paste, whereas VC (vibrated concrete) is the toughest, caused by the larger amount of coarse aggregates and the more prominent interlocking mechanism during fracture. Indeed, the smallest fracture parameters are found for SCC1 in case of the 3PBT and the largest ones occur for VC in the WST. Hence, it seems that the outcome of the 3PBT strongly depends on the cement paste strength, while the results of the WST are dominated by the amount of bridging elements (i.e. coarse aggregates). These differences between the two test setups may be attributed to the dissimilar specimen size, shape, and self-weight, a diverse length of the fracture process zone (FPZ), a varying stress state near the crack, and the potential storage of elastic energy during testing.
As a direct consequence, SCC1 performs worst in the dynamic 3PBTs and VC can sustain the most load cycles to failure (for the load ranges 10–80%, 10–75%, and 10–70%), when considering the WSTs. SCC2 (with equal w/c ratio as VC), which has the largest compressive strength of the three batches, has the highest overall fatigue resistance in the 3PBTs and also in case the load level 10–90% is applied in the WSTs. So, at first sight, the fatigue performance and the cracking behaviour of concrete under cyclic loading appears to depend on the static compressive strength. However, this conclusion cannot be stated with certainty, since scatter is present in the results of the dynamic experiments due to the inevitable spread in the strength of different samples, which is caused by the heterogeneous nature of concrete.
When comparing the fracture parameters, based on the experimentally determined load–CMOD curves (load versus crack mouth opening displacement), and the numerical ones, derived from inverse analysis, large differences are noticed. The tensile strength is, in general, overestimated by the computation software, and even the mutual relationship between VC, SCC1, and SCC2 is altered. Considering Young's modulus, a substantial deviation is present, except for SCC1, for which the estimation of the experimental value is quite good in both the 3PBT

and the WST. Regarding the characteristic length, the best correspondence is found for the WST, whereas the fracture energy is best approached in case of the 3PBT.

Acknowledgments

The authors wish to express their gratitude to all the students who assisted in the preparation and implementation of the tests. The research fund University College Ghent is thankfully acknowledged for the financial support, and OBC-Ottevaere for the delivery of the concrete.

References

[1] Jenq Y-S, Shah SP. Features of mechanics of quasi-brittle crack propagation in concrete. Int J Fract 1991;51:103–20.
[2] Bazant ZP. Fracture mechanics of concrete structures. London: Taylor & Francis; 2005.
[3] Hanjari KZ. Evaluation of WST method as a fatigue test for plain and fiberreinforced concrete (master's thesis). Göteborg: Chalmers University of Technology; 2006.
[4] De Schutter G, Bartos P, Domone P, Gibbs J. Self-compacting concrete. Caithness: Whittles Publishing; 2008.
[5] De Schutter G, Audenaert K. Durability of self-compacting concrete. In: RILEM, Report 38; 2007.
[6] De Schutter G, Boel V. Self-compacting concrete. In: Proceedings of the fifth international RILEM symposium on SCC. RILEM Publications; 2007.
[7] Domone PL. A review of the hardened mechanical properties of selfcompacting concrete. Cem Concr Compos 2007;29:1–12.
[8] Issa MA, Hammad AM, Chudnovsky A. Correlation between crack tortuosity and fracture toughness in cementitious material. Int J Fract 1993;60:97–105.
[9] de Oliveira e Sousa JLA, Bittencourt TN. Experimental analysis of fracture processes in concrete. J Brazilian Soc Mech Sci 2001;23(4):545–50.
[10] CEN. EN 12350-7. Testing fresh concrete; part 7; 2009. [11] CEN. EN 12350-2. Testing fresh concrete; part 2; 1999.
[12] CEN. EN 12350-5. Testing fresh concrete; part 5; 1999. [13] CEN. EN 12350-8. Testing fresh concrete; part 8; 2007.
[14] CEN. EN 12350-9. Testing fresh concrete; part 9; 2007.
[15] CEN. EN 12390-3. Testing hardened concrete; part 3; 2001.
[16] CEN. Eurocode EN. Design of concrete structures: general rules and rules for buildings; 2004.
[17] NBN. B15-203. Proeven op beton: Statische elasticiteitsmodulus bij druk; 1990.